INTERNATIONAL JOURNAL FOR NUMERICAL METHODS IN FLUIDS, VOL. 16, 403 419 (1993)

COMPARISON OF SEVERAL OPEN BOUNDARY NUMERICAL TREATMENTS FOR LAMINAR RECIRCULATING FLOWS

M. H. KOBAYASHI, J. C. F. PEREIRA AND J. M. M. SOUSA

Instituto Superior Técnico/Technical University of Lisbon, Mechanical Engineering Department, Av. Rovisco Pais, 1096 Lisboa Codex, Portugal

SUMMARY

Several open boundary conditions (OBCs) are compared and evaluated in the framework of the SIMPLE algorithm using staggered and non-staggered grid systems. The benchmark laminar flow test cases used for the OBC evaluation are Poiseuille–Benard flow in a channel and stratified backward-facing step flow. The investigated OBCs are linear explicit step space extrapolation, Orlanski's monochromatic wave, and pressure extrapolation. Orlanski's and pressure extrapolation open boundary treatment for unsteady and steady flows, respectively, yield little reflection and has proved to be adequate for engineering calculations.

KEY WORDS Outflow boundary conditions Laminar recirculating flows Non-staggered grid systems

INTRODUCTION

Most CFD simulations of real fluid flow problems are sought in a computational domain that only overlaps the physical domain in a very small region. This is achieved by introducing one (or several) open boundary conditions (OBCs) at some arbitrary finite distance. As there is no fluid-dynamic information outside of the computational domain, flow modelling assumptions are made at the boundary location and are dependent upon the physical problem and the mathematical character of the governing equations.

For problems governed by hyperbolic systems of equations, a large amount of fundamental studies have been conducted, aiming to analyse the OBC influence on the global accuracy of the difference approximation.[1,2] Several non-reflecting OBCs have been developed to permit the phenomena generated in the domain to pass through the boundary without undergoing significant distortion and without influencing the interior solution.[3–6]

Calculations of incompressible fluid flow, comprising regions dictated by elliptic character of the governing equations, usually have the outflow boundary located too far from the region where the solution is sought. The argument is that, far from the artificial boundary, the solution will be negligibly contaminated by inherent modelling or numerical errors due to the prescribed Dirichlet or von Newman type of boundary condition. Dekruif and Hassan[7] investigated the implications of truncating semi-infinite physical domains on the accuracy of the solutions of laminar flow past a flat plate with a forward-facing step. The truncated physical domain yields inaccurate solutions compared to those obtained in a mapped plane. Shyy[8,9] investigated the influence of von Newman conditions for several flows, including the simultaneous presence of inflow and outflow through the open boundary. For flows with multiple recirculating eddies

0271–2091/93/050403–17$13.50

Received 22 November 1991
Revised 6 August 1992

across the open boundary, the numerical stability of the computations was related to the Reynolds number. In addition, waves generated by the numerical procedure were reflected at the boundary. A partial cure to reduce numerical reflections at the boundaries to a negligible order is the use of Sommerfeld-type of radiation conditions.[1] This method assumes a travelling wave that is convected through the open boundary. Different implementations of the method were performed[10-12] by investigating the implications of different wave equation discretization schemes, or procedures to estimate phase speed, etc.

A common remark of previous investigations using primitive variable formulation is the sensitivity of the results to pressure open boundary conditions.[9,10] This is of particular relevance due to a large number of finite volume computations being performed using the SIMPLE[13] family of pressure–velocity algorithms, with staggered grid systems, and also due to the increasing popularity of non-staggered grid systems, using pressure-weighted interpolation method.[14,15]

The main objective of this work is to compare several numerical treatments of open boundary conditions, incorporated in SIMPLE algorithms with special emphasis to non-staggered grid systems. The selected flow cases correspond to Poiseuille–Bénard flow in a channel (see Figure 1(a)) and stratified flow over a backward-facing step (see Figure 1(b)). These flows were predicted by Evans and Paolucci[16] and Leone,[17] respectively, and their predictions are used as benchmark solutions.

NUMERICAL ALGORITHMS

Flow equations

Assuming a planar, two-dimensional, laminar flow of a Newtonian fluid induced by buoyancy forces (using the Boussinesq approach), the Navier–Stokes equations, continuity equation and

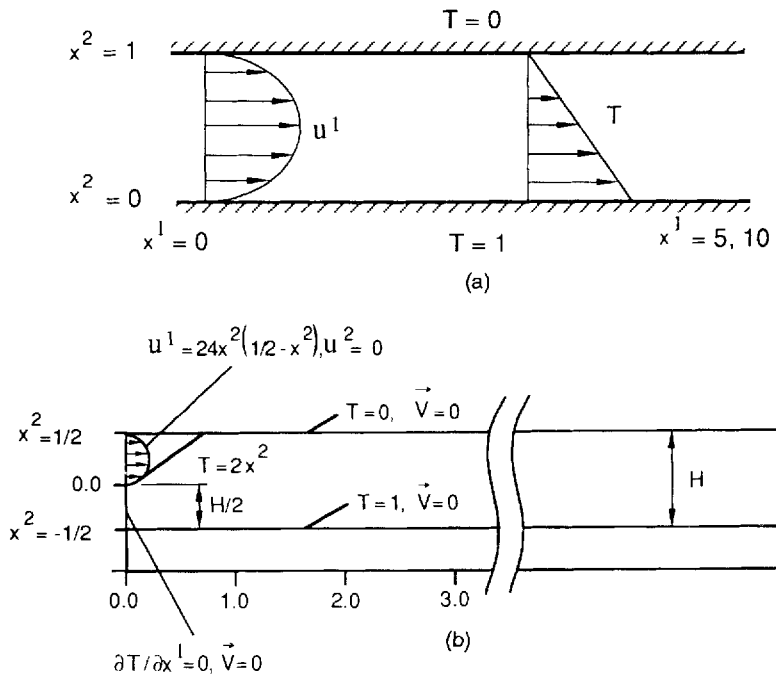

Figure 1. Computational domains and boundary conditions: (a) Poiseuille–Bénard flow in a channel; (b) stratified backward-facing step

energy conservation equation can be expressed in non-dimensional vectorial notation as follows:

continuity

$$\nabla \cdot \mathbf{v} = 0, \tag{1}$$

momentum equation

$$\frac{\partial \mathbf{v}}{\partial t} + \nabla \cdot (\mathbf{v} \otimes \mathbf{v}) = -\nabla p + Re^{-1} \nabla^2 \mathbf{v} + Fr^{-1} T\mathbf{k}, \tag{2}$$

energy equation

$$\frac{\partial T}{\partial t} + \nabla \cdot (\mathbf{v} T) = Pe^{-1} \nabla^2 T, \tag{3}$$

where $\mathbf{v}$ is the velocity vector, p is the static pressure, T is the temperature and $\mathbf{k}$ is the upward vertical unit vector, $Re \equiv \bar{u}_{1\,\mathrm{in}}\, H/v$ is the Reynolds number and $Fr \equiv (\bar{u}_{1\,\mathrm{in}}/u_{1\,\mathrm{B}})^2$ is the Froude number. Here $\bar{u}_{1\,\mathrm{in}}$ is the average inlet velocity, H is the height of the channel, $u_{1\,\mathrm{B}} = NH$ is the buoyancy velocity, with $N \equiv (\beta g \Delta T/H)^{1/2}$ standing for the Brunt–Vaisala frequency; β is the volumetric expansion coefficient and g is the acceleration due to gravity. These equations may be cast in a form of the general transport equation which is used for discretization purposes:

$$\frac{\partial \phi}{\partial t} + \frac{\partial}{\partial x^j}\left(u_j \phi - \Gamma \frac{\partial \phi}{\partial x^j} \right) = S_\phi, \tag{4}$$

where $\phi = (u_i, T)$, u_i being the velocity component in the x^i Cartesian direction, $\Gamma = (Re^{-1}, Pe^{-1})$ and S_ϕ stands for the pressure gradient and the buoyancy force.

Discretization procedure

The flow equations are discretized using a finite-volume method. First, equation (4) is integrated over the control volume and time step:

$$\int_{\mathrm{s}}^{\mathrm{n}} \int_{\mathrm{w}}^{\mathrm{e}} \int_{t}^{t+\Delta t} \frac{\partial \phi}{\partial t}\, \mathrm{d}t\, \mathrm{d}x^1\, \mathrm{d}x^2 + \int_{t}^{t+\Delta t} \left\{ \int_{\mathrm{s}}^{\mathrm{n}} \int_{\mathrm{w}}^{\mathrm{e}} \frac{\partial J_i}{\partial x^i}\, \mathrm{d}x^1\, \mathrm{d}x^2 \right\} \mathrm{d}t = \int_{t}^{t+\Delta t} \int_{\mathrm{s}}^{\mathrm{n}} \int_{\mathrm{w}}^{\mathrm{e}} S_\phi\, \mathrm{d}x^1\, \mathrm{d}x^2\, \mathrm{d}t, \tag{5}$$

where J_i stands for the convective and diffusive fluxes in the x^i direction.

Two numerical algorithms were used. The first employs the Euler implicit temporal discretization, i.e. equation (5) becomes, after integration using the Gauss theorem,

$$(\phi^{n+1} - \phi^n)\Delta x^1 \Delta x^2 + \left[\left(u_1 \phi - \Gamma \frac{\partial \phi}{\partial x^1} \right)_{\mathrm{e}}^{n+1} - \left(u_1 \phi - \Gamma \frac{\partial \phi}{\partial x^1} \right)_{\mathrm{w}}^{n+1} \right] \Delta x^2 \Delta t$$

$$+ \left[\left(u_2 \phi - \Gamma \frac{\partial \phi}{\partial x^2} \right)_{\mathrm{n}}^{n+1} - \left(u_2 \phi - \Gamma \frac{\partial \phi}{\partial x^2} \right)_{\mathrm{s}}^{n+1} \right] \Delta x^1 \Delta t = \bar{S}_\phi^{n+1}, \tag{6}$$

where $\bar{S}_\phi^{n+1}$ is the averaged source term.

The 13-point QUICK scheme[18, 19] is used for convection discretization, while central differences approximation is used for diffusion terms. For example, ϕ_{w} is approximated by

$$\phi_{\mathrm{w}} = a_0 + a_1 \frac{\Delta x^1}{2} + a_2 \left(\frac{\Delta x^1}{2} \right)^2 - a_4 \frac{1}{3} \frac{(c_y^3 + 1)}{(c_y + 1)^3} \left(\frac{\Delta x^2}{2} \right)^2, \tag{7}$$

where c_y takes into account the grid non-uniformity in a staggered grid and is equal to 1 for

a non-staggered one. Coefficients a_j are obtained from the assumption of a quadratic surface:

$$\phi = a_1 + a_2\xi + a_3\xi^2 + a_4\eta + a_5\eta^2 + a_6\xi\eta. \tag{8}$$

A staggered grid system is used together with the standard (in the local reference frame (ξ, η) oriented with the velocity components) SIMPLE algorithm to correct the velocity field and to calculate the pressure field.

The second algorithm employs non-staggered grids, where all variables are stored in the same place, at the centre of the control volume (CV). Finite difference equations are derived by integration of equation (4), with $\partial\phi/\partial t = 0$, over the respective CV. The convective flux is evaluated by using the non-symmetric second-order upwind scheme and the Pressure-Weighted Interpolation Method (PWIM). These approaches lead to the following equation, e.g. for the 'e' face:

$$J_{1e}^{c} = u_{1e}\phi_e, \tag{9}$$

where

$$\begin{aligned} \phi_e &= \phi_E + (\phi_E - \phi_{EE}) fx_E^1 \qquad \text{if } u_{1e} \le 0, \\ \phi_e &= \phi_P + (\phi_P - \phi_E)(1 - fx_W^1) \qquad \text{if } u_{1e} > 0, \end{aligned} \tag{10}$$

where J_1^c is a convective flux and fx^1 is the linear interpolation factor which takes into account the grid non-uniformity. Fluxes through other faces are calculated similarly.

When using a staggered grid system, the convective fluxes are evaluated directly, since the velocity components are stored at the CV faces. For non-staggered grids the u_i-momentum equations are arranged in the form

$$\begin{aligned} u_{iP} &= H^i(u_{im}) - (Q^i \delta^i p)_P - Su_i^P + (1-\alpha)u_{iP}^n, \\ u_{iC} &= H^i(u_{im}) - (Q^i \delta^i p)_C - Su_i^C + (1-\alpha)u_{iC}^n \end{aligned} \tag{11}$$

as obtained from the application of the finite-difference equation at point P and at a surrounding point $C = E, W, N, S$. At control volume face c between points C and P, the velocity value is given by

$$u_{ic} = \overline{H^i(u_{im})} - (Q^i \delta^i p)_c + \overline{Su_i} + (1-\alpha)u_{ic}^n, \tag{12}$$

where the operators H^i and Q^i are defined by

$$H^i(u_{im}) = \sum \frac{a_{im} u_{im}}{a_P^{u_i}}, \tag{13}$$

$$Q^i = \frac{A_i}{a_P u_i}.$$

Here A_i is the area of the control volume faces, a_{im} and $a_P^{u_i}$ are the finite-difference coefficients representing the convection and diffusion contribution in the discretized momentum equations; the overbar denotes linear interpolation. Pressure gradient is computed explicitly in equation (12) to ensure pressure–velocity coupling. This procedure for pressure–velocity coupling can be used with all algorithms of the SIMPLE family.

Pressure–velocity coupling

Due to the OBC influence on pressure field, the basic SIMPLE algorithm is briefly outlined for a better understanding of the results presented in this paper. The algorithm is common to staggered or non-staggered grids.

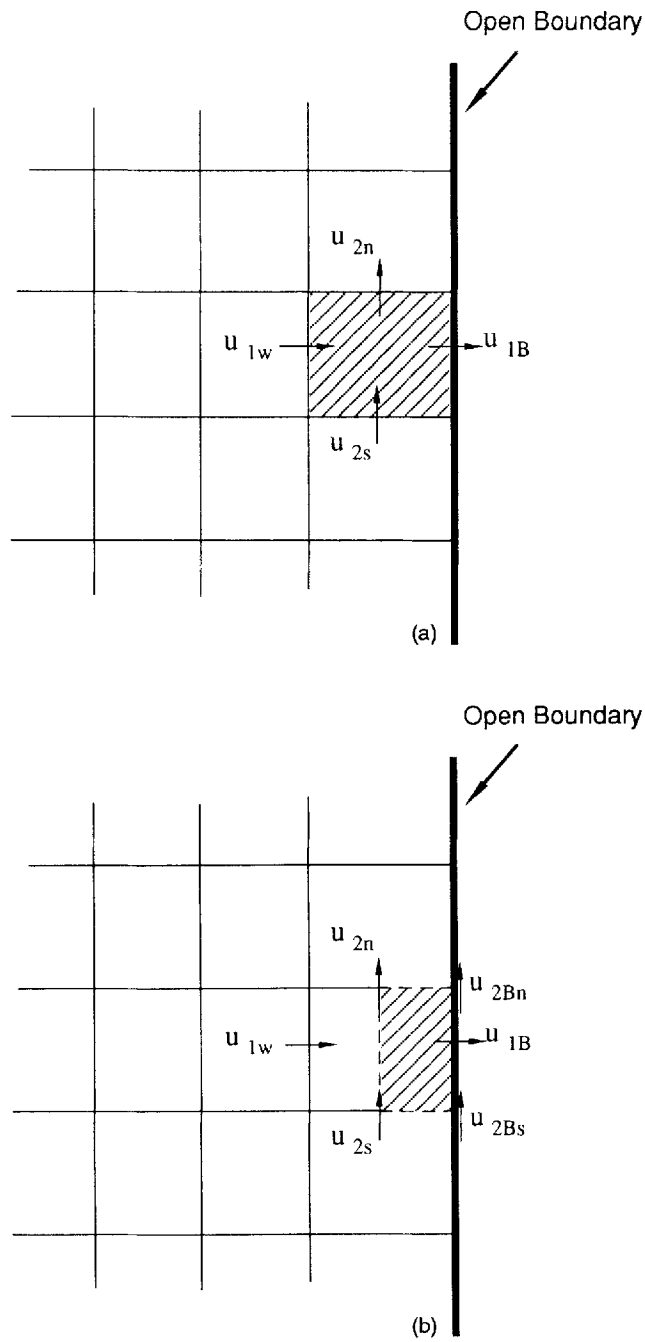

Figure 2. Grid system. Continuity equation is only applied to the shaded area for OBC2: (a) staggered grid: u_1-momentum equation; (b) staggered grid; u_2-momentum equation

After the momentum equations have been solved, a velocity field u_i^* is obtained. The combination of momentum and continuity equations, under the assumption that ($p^* = p + p'$ and $u^{**} = u_i^* + u_i'$), yields the derivation of a velocity correction as a function of the pressure correction:

$$u_i' = Q_i \delta' p' \tag{14}$$

and using u^{**} in the continuity equation yields the following pressure correction equation:

$$a_P p_P' = \sum a_{nb} p_{nb}' + S_m, \tag{15}$$

where nb = E, W, N, S and S_m is given by mass balance

$$S_m = u_{1e}^* \Delta x^2 - u_{1w}^* \Delta x^2 + u_{2n}^* \Delta x^1 - u_{2s}^* \Delta x^1. \tag{16}$$

In order to improve convergence, an under-relaxation factor, α_P, is introduced, yielding the following equation for u_i':

$$u_i' = Q_i \frac{\delta' p'}{\alpha_P}. \tag{17}$$

The value of α_P is equal to 1 for staggered grids and 0·8 for non-staggered grids. After solving the pressure correction equation, u_1, u_2 and p are updated. The coefficients of the energy conservation equation are solved to obtain the temperature field and this outer cycle is repeated until convergence criteria are satisfied. An inner cycle to solve the algebraic system of equations is performed using the strongly implicit scheme; see References 20 and 21.

Open boundary conditions

The following OBC numerical treatments were used:

OBC1: An explicit step space extrapolation using explicit one-sided difference to approximate a zero first derivative along the main flow direction, $\phi_B^{n+1} = \phi_P^n$.

OBC2: Mass conservation at half-CV. The outflow boundary condition for u_1-velocity was given by mass conservation (see Figure 2(a)):

$$u_{1B}^{n+1} = (u_{2s}^n \Delta x^1 - u_{2n}^n \Delta x^1 + u_{1w}^n \Delta x^2)/\Delta x^2. \tag{18}$$

The open boundary condition treatment for u_2-velocity was evaluated from mass balance at half-CV (see Figure 2(b)):

$$\frac{\Delta x^1}{8} u_{2Bs}^{n+1} - \left(\frac{3}{4} u_{2s}^n + \frac{1}{4} u_{2Bn}^{n+1}\right) \frac{\Delta x^1}{2} + \left[u_{1B}^n \Delta x^2 - \frac{1}{2}(u_{1B}^n + u_{1w}^n)\Delta x^2\right] + \frac{3}{4} u_{2n}^n \frac{\Delta x^1}{2} = 0. \tag{19}$$

At the lower solid wall, u_{2Bs} is equal to zero and u_{2Bn} can be calculated explicitly using equation (19). This procedure is applied recursively to obtain all the values of u_2 at the outlet boundary.

OBC3: A monochromatic travelling wave, Orlanski[1] boundary condition

$$\frac{\partial \phi}{\partial t} + c \frac{\partial \phi}{\partial x^1} = 0 \tag{20}$$

was assumed at the boundary with prescribed wave speed as the mean channel velocity, $c = \overline{u_1}$, yielding

$$\phi_B^{n+1} = \phi_B^n - \frac{\bar{u}_{1in} \Delta t}{\Delta x^1} (\phi_B^n - \phi_P^n), \qquad \phi = u_i, T. \tag{21}$$

OBC4: Explicit step space extrapolation using linear extrapolation from two interior grid nodes.

OBC5: This boundary condition was specially developed to be used with non-staggered grid arrangement. A linear profile for the outflow pressure field is assumed, i.e.

$$p_B = p_P + (p_P - p_W)(1 - f x^1_W). \tag{22}$$

However, for the boundary velocity correction, if the velocity is simply extrapolated from the interior nodes, mass will not be conserved, and if equation (17) is used, instabilities will propagate upstream and divergence may occur. On the other hand, if the velocity is extrapolated from interior nodes to conserve mass, u'_{ic} at boundary is zero and no information from the boundary is needed. In this case the velocity will depend on the pressure only from the momentum equation and a weighting pressure must be used in order to prevent instabilities. In this work the following alternative boundary condition is used.

The mass boundary lies half-way in the middle of the control volume, so, the mass balance for the CV reads

$$\rho u^{**}_{1P} \Delta x^2 - \rho u^{**}_{1w} \Delta x^2 + \frac{\rho u^{**}_{2n} \Delta x^1}{2} - \frac{\rho u^{**}_{2s} \Delta x^1}{2} = 0, \tag{23}$$

where u'_{iP} is naturally linked to the prescribed $p'_E = 0$ at exit by the following equation:

$$u'_{iP} = \frac{1}{a_P}(p'_B - p'_P).$$

As can be seen from equations (11), (23) and (24), velocity at point P is related to the outlet pressure via both momentum and pressure correction equations. This procedure enhances the pressure velocity coupling, thus improving the robustness and the convergence properties of the method.

RESULTS AND DISCUSSION

Poiseuille–Bénard flow in a channel

Numerical predictions were obtained for the following values of relevant parameters: $Re = 10$, $Fr = 1/150$ and $Pr = 2/3$, for the geometry depicted in Figure 1(a). The computational grid was uniform in both co-ordinate directions $[\Delta x^1, \Delta x^2] = [0{\cdot}1, 0{\cdot}04]$, containing 102×27 control volumes and covering the computational domain up to $x^1 = 10$. An Euler implicit temporal discretization with a time step $\Delta t = 0{\cdot}055\sqrt{Fr}$ was used, together with the QUICK scheme for space discretization.

Figure 3(a) shows the streamlines obtained with OBC1, corresponding to time t_T when a minimum in temperature occurs at the location $x^1 = 5{\cdot}0$, $x^2 = 0{\cdot}5$ (see Figure 3(b)). Figure 3(c) shows the location of the velocity components maxima at t_T. The figures show the start-up region as well as the flow region affected by the incorrect outflow conditions. The velocity field corruption at the boundary has propagated four vertical channel heights upstream of the outflow.

Table I shows the flow parameters obtained using OBC3 and those reported by Evans and Paolucci[16] using a similar space and time increments $[\Delta x^1, \Delta x^2, \Delta t] = [0{\cdot}1/\sqrt{2},\ 0{\cdot}05/\sqrt{2},\ 0.05\sqrt{Fr}]$. The results show good agreement despite the fact that they have considered a much longer computational domain, up to $x^1 = 20$. Small differences in the mean flow parameters may arise due to the relative weight of the affected values, close to outflow boundary.

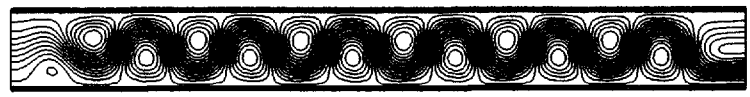

(a)

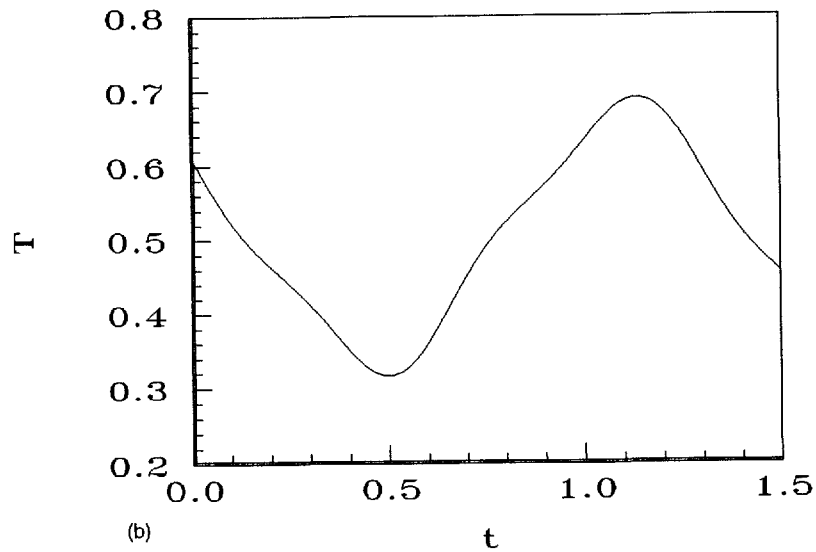

(b)

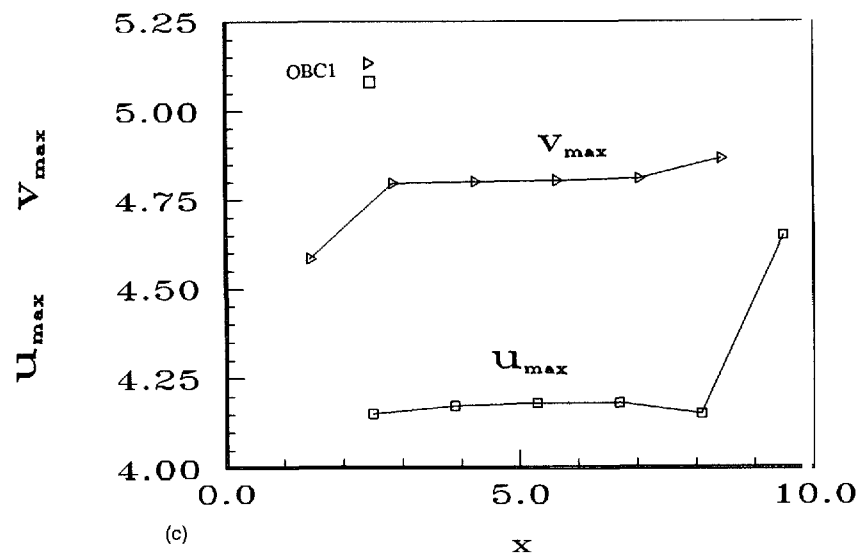

(c)

Figure 3. Results for the computational domain up to $x^1 = 10$: (a) streamline contours at t_T; (b) temperature minimum in time, $t_T = 0{\cdot}5$; (c) velocity components maxima at t_T

Table I. Evaluation of flow parameters obtained with OBC3 located at $x^1 = 5$, and comparison with reference values

	τ	λ	$\langle \overline{Nu} \rangle$	$u_{1\max}$	x^2 $u_{1\max}$	$u_{1\min}$	x^2 $u_{1\min}$	$u_{2\max}$	x^2 $u_{2\max}$	$u_{2\min}$	x^2 $u_{2\min}$
OBC3	1·283	$1{\cdot}4\ ^{-0{\cdot}013}_{+0{\cdot}146}$	2·576	4·183	0·82	−2·566	0·14	4·806	0·54	−4·874	0·50
Evans and Paolucci[16]	1·290	1·400	2·568	4·211	0·803	−2·613	0·138	4·950	0·51	−4·951	0·49

To avoid any confusion between convective or temporal discretization errors and the specific outflow numerical treatments, the following strategy was employed. Any accurate OBCs should give a solution equal to the one obtained at the same location but with the outflow section located far downstream. So, first we calculate the flow up to $x^1 = 10$ using 102×27 control volumes; Secondly, calculations are performed with the outflow located at $x^1 = 5$ and using the equivalent number of grid nodes (51×27); the dependent variables (u_i, p, T) calculated at $x^1 = 5$ using the large domain are assumed to be the benchmark solutions to compare with those calculated when the outflow coincides with this plane ($x^1 = 5$).

Figures 4(a)–4(e) show the field plots of velocity vectors, streamlines, vorticity, pressure and temperature contours, respectively. Each figure shows four plots, the first, denoted as EXACT, obtained in a computational domain $x^1 \in [0, 10]$ displaying only to $x^1 = 5$ (see Figure 3(a)). The other three plots correspond to OBC1, OBC2 and OBC3 numerical treatments. All the figures were obtained at time $t = t_T$. The absolute value of this time is arbitrary, since the rolls are convected downstream. The results show that large differences exist between the solutions for various OBCs. The corrupted flow resulting from OBC1 reaches the start-up region. The length of the region affected by outflow boundary conditions can be seen more clearly in Figure 5. The monochromatic travelling wave, OBC3, yields results closer to the benchmark solution, but still does not ensure full transmission of all waves at the boundary. However, the local wave speed, assumed to be equal to the mean bulk velocity, is 8% in error compared to the calculated wavelength and wave period. The implementation of OBC4, using linear extrapolation for temperature, did not improve the results because the temperature distribution displays a minimum in the OBC location, at $t = t_T$, as mentioned before.

Velocity profiles at the boundary, $x^1 = 5$, are shown in Figure 6(a) and the calculated stream-function and temperature distribution in Figures 6(b) and 6(c), respectively. OBC1 is clearly erroneous. OBC2 ensures the incompressible condition for velocity at half-control volume face close to the outflow and, therefore, an improvement in the velocity field was obtained. The results shown by OBC3 yield the best results among the implemented OBC treatments, in agreement with the previous results.[22]

The Poisson equation for pressure correction embodied in the SIMPLE algorithm does not require special care in the specification of boundary conditions. Pressure correction is zero when velocity is prescribed such as inlet, walls or outflow conditions. Several other finite-difference methods, e.g. MAC, pseudo-compressibility, fractional-step or projection methods and other methods, express pressure directly in terms of a Poisson equation replacing the mass conservation equation. The implications and selection of boundary conditions have been discussed; see References 23–26. However, the similarities between the two procedures say, the SIMPLE algorithm and the pressure Poisson equation for incompressible flows has not been extensively addressed.[26] When the SIMPLE algorithm is used, the implied boundary condition for a pressure Poisson equation at an outflow portion of the domain should be found by solving the pressure

gradient from the momentum equation using the calculated velocity field. The opposite is also true, given a converged solution using the SIMPLE algorithm: the implied gradient pressure condition at the outflow may be obtained from the pressure Poisson equation.

Stratified flow over a backward-facing step

The second test case corresponds to the stratified flow over a backward-facing step proposed by Leone[17] (see Figure 1(b)). The governing flow parameters are the same as in Leone's work, i.e. $Pr=1$, $Fr=16/9$ and $Re=800$. These numbers yield a value of $3{\cdot}6\times10^5$ for the Grashof

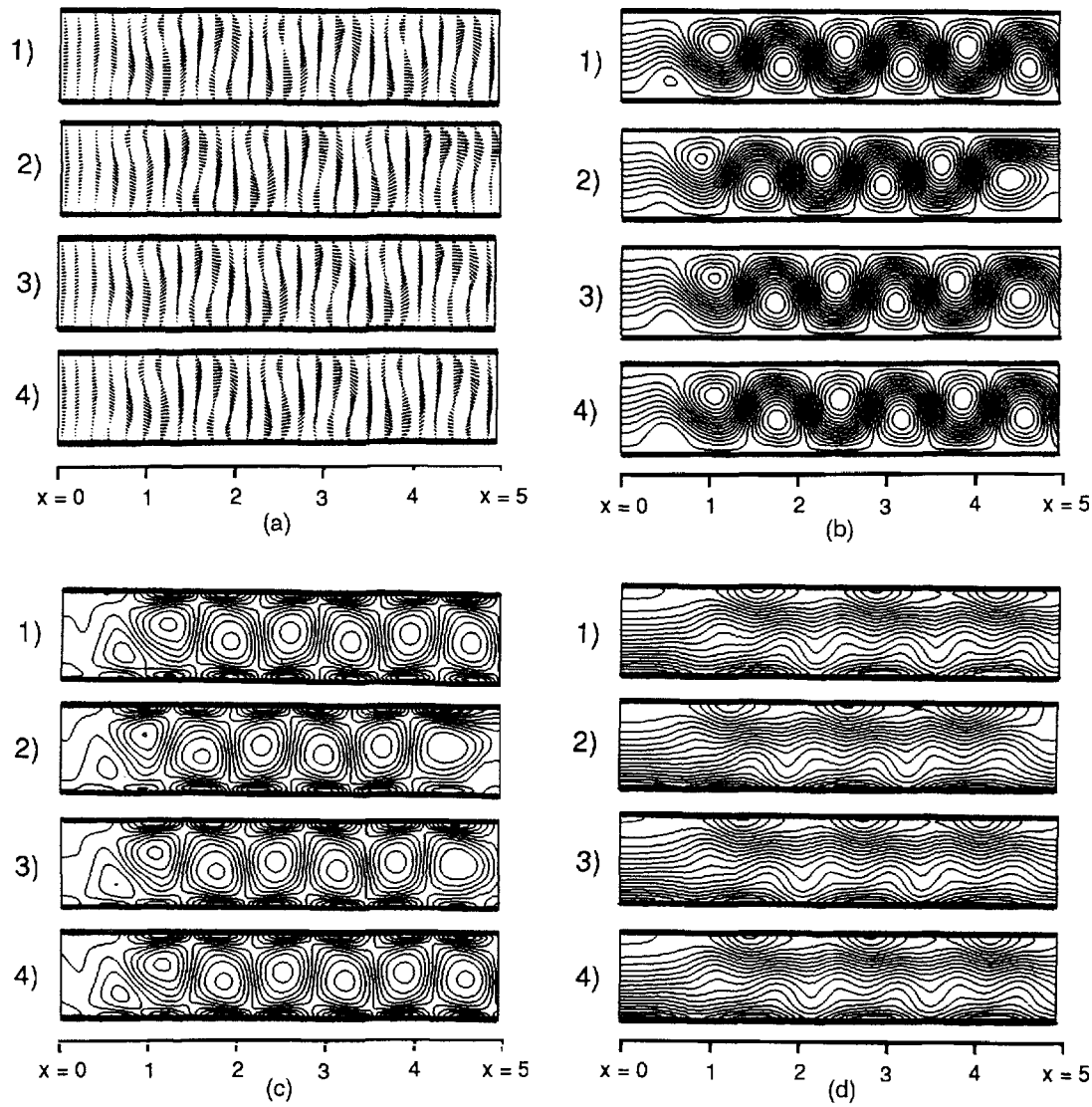

Figure 4. Field plots at t_T, for the different OBC treatments: (1) OBC at $x=10$, exact solution; (2) OBC1; (3) OBC2; (4) OBC3. (a) velocity vectors; (b) streamlines; (c) vorticity contours; (d) pressure contours; (e) temperature contours

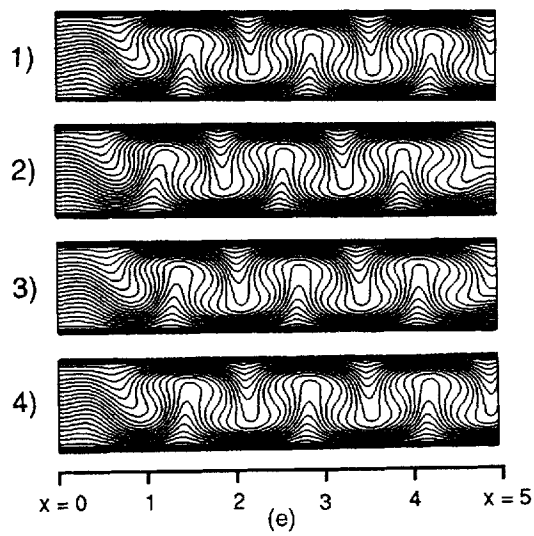

Figure 4. (Continued)

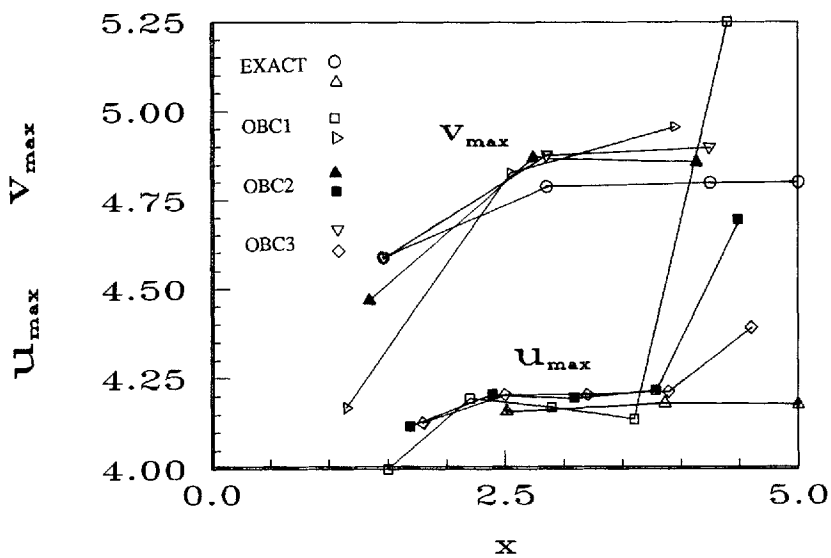

Figure 5. Velocity components maxima for the different OBC treatments

($Gr = Re^2/Fr$) and Rayleigh ($Ra = Pr\ Gr$) numbers. As in the previous sections, computations have been carried out for a longer and a shorter domain corresponding to $x^1_{max} = 15$ and $x^1_{max} = 7$, respectively (cf. Figure 1(b)).

Figure 7 shows the streamlines and isothermal maps obtained using the proposed open boundary condition for $x^1_{max} = 15$. The main flow features, viz. the positions and strengths of the eddies, as well as the temperature distribution, are well predicted. The streamlines and temperature contours, using the same contour values as in Figure 7, are shown in Figure 8 for $x^1_{max} = 7$.

These results indicate good agreement between the present predictions and the solutions obtained by Leone.[17]

Table II lists the locations, sizes, strengths and positions of streamfunction maxima for the five eddies. A comparison of the predicted values and the reference values indicates that the strengths, positions and lengths of the eddies are well predicted. Table III presents the differences between

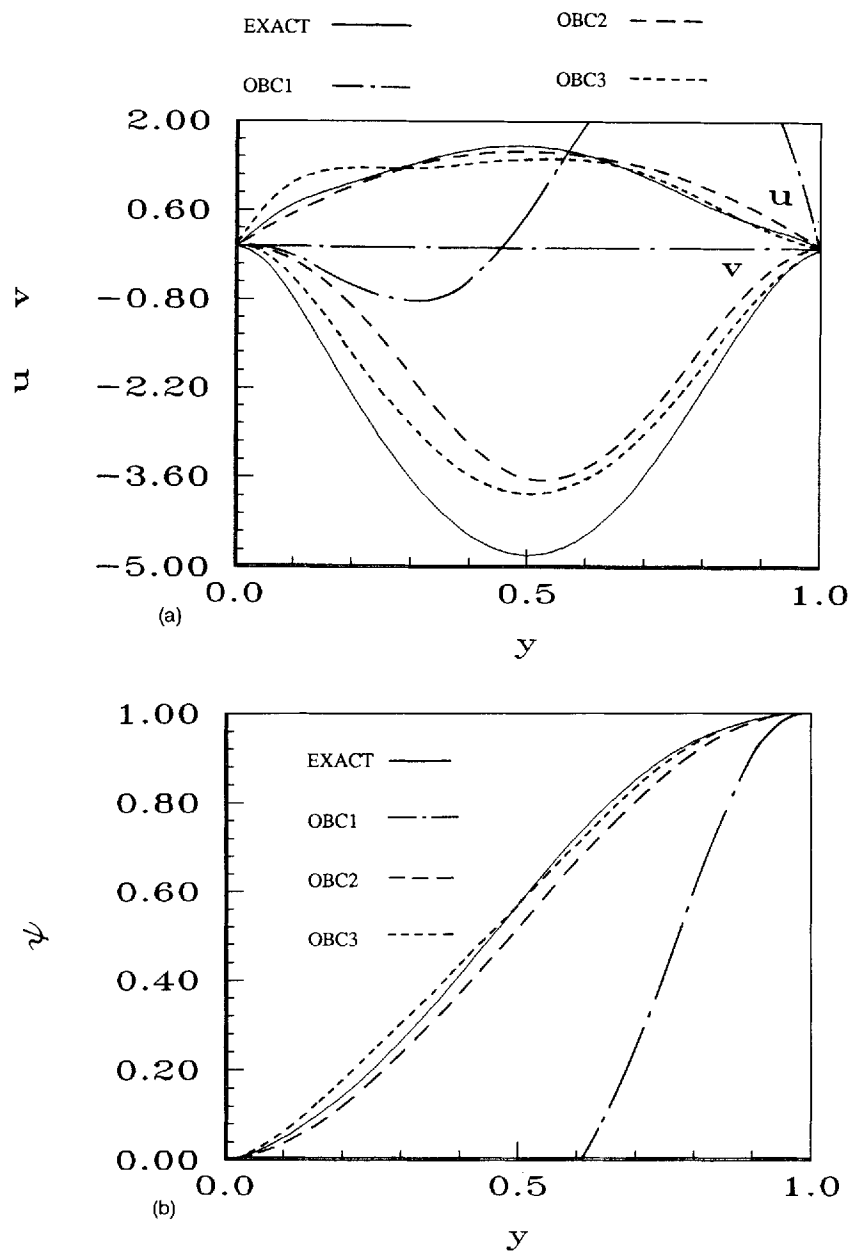

Figure 6. Transverse profiles at outlet boundary for the different OBC treatments: (a) velocity components; (b) streamfunction; (c) temperature

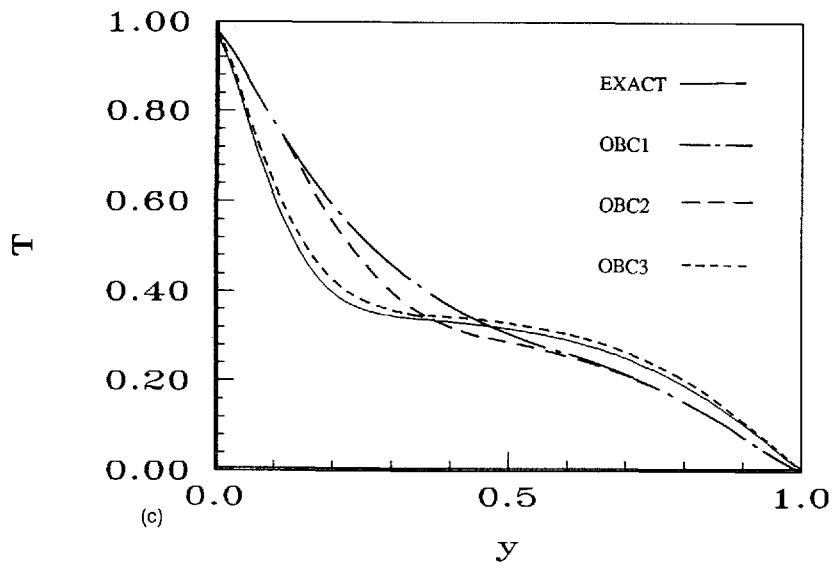

Figure 6. (Continued)

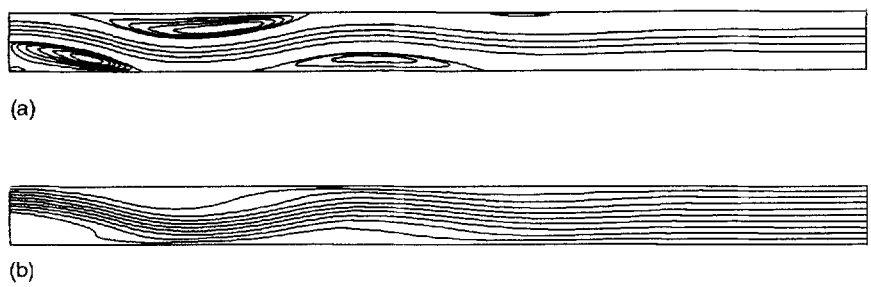

Figure 7. Steady-state contours for $x^1_{max} = 15$: (a) streamlines; (b) temperature contours

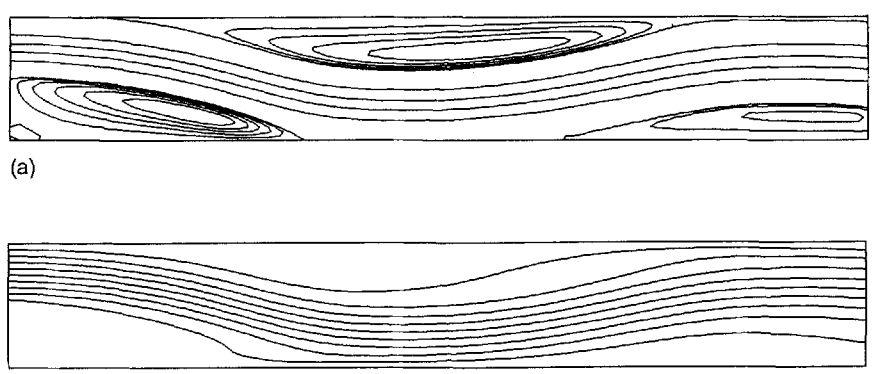

Figure 8. Steady-state contours for $x^1_{max} = 7$: (a) streamlines; (b) temperature contours

long- and short-domain results for the items listed in Table II. As can be seen from this table, the differences between the results obtained using shorter or larger domains are very small compared to the differences between them and the reference values. This fact clearly indicates the insensitivity of the predictions using OBC5 on the position of the outlet station.

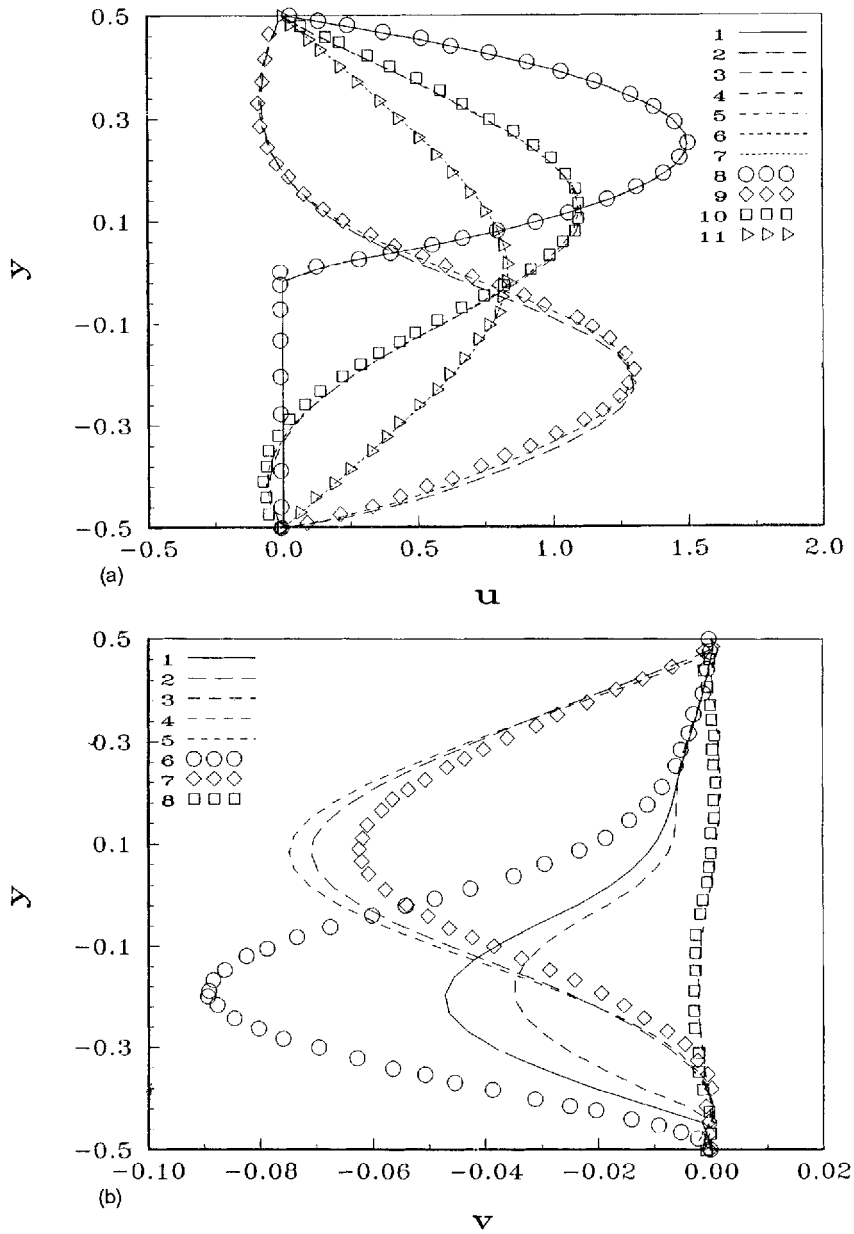

Figure 9. Transverse profiles. (a) u_1-velocity: (1) $x^1_{max}=7$, $x^1=0$; (2) $x^1_{max}=7$, $x^1=3$; (3) $x^1_{max}=7$, (4) $x^1_{max}=15$, $x^1=0$; (5) $x^1_{max}=15$, $x^1=3$; (6) $x^1_{max}=15$, $x^1=7$; (7) $x^1_{max}==15$, $x^1=15$; (8) Leone^{17}, $x^1=0$; (9) Leone^{17}, $x^1=3$; (10) Leone^{17}, $x^1=7$; (11) Leone^{17}, $x^1=15$; (b) u_2-velocity: (1) $x^1_{max}=7$, $x^1=3$; (2) $x^1_{max}=7$, $x^1=7$; (3) $x^1_{max}=15$, $x^1=3$; (4) $x^1_{max}=15$, $x^1=7$; (5) $x^1_{max}=15$, $x^1=15$; (6) Leone^{17}, $x^1=3$; (7) Leone^{17}, $x'=7$; (8) Leone^{17}, $x^1=15$; (c) temperature (see Figure 9(a)); (d) vorticity (see Figure 9(a))

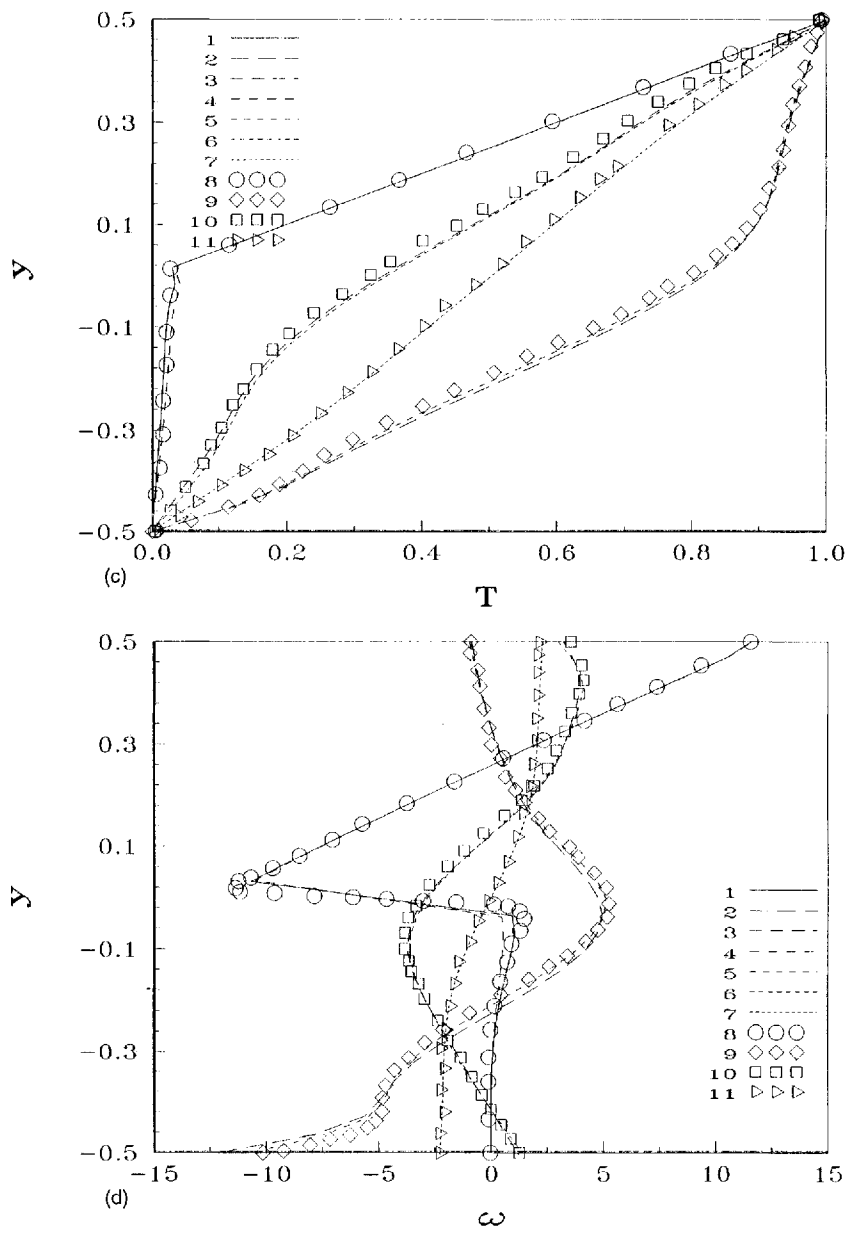

Figure 9. (Continued)

Finally, Figure 9 shows transverse profiles of velocity, temperature and vorticity. The close agreement between predictions and reference values, for both short- and long-domain solutions, indicates that the overall resolution of the flow field is adequate. The only difference in the transverse velocity component at $x^1 = 3$ represents less than 5% of the reference velocity and has no consequence on the solution field since it is one order of magnitude smaller than the streamwise velocity component (see Figure 9(d)). Here we should note that the transverse velocity discussed here cannot be predicted at all by using the commonly adopted OBC1 (cf. Figure 6(a)).

Table II. Comparison of eddy positions and lengths with reference values using OBC5 for $x^1_{max}=7$ and $x^1_{max}=15$

Eddy		Start x^1	Stop x^1	Length	Maximum value	x^1-co-ordinate	x^2-co-ordinate
1 (bottom)	$x_{max}=7$	0	0·255	0·255	0·00004	0·0778	−0·4286
	$x_{max}=15$	0	0·284	0·284	0·00003	0·1570	−0·4328
	Leone[17]	0	0·356	0·356	0·00008	0·0125	−0·4000
2 (bottom)	$x_{max}=7$	0·255	2·349	2·094	−0·02247	1·478	−0·2857
	$x_{max}=15$	0·284	2·270	1·986	−0·02609	1·414	−0·2942
	Leone[17]	0·356	2·498	2·142	−0·02239	1·500	−0·2625
3 (bottom)	$x_{max}=7$	4·303	—	—	−0·00748	6·611	−0·3214
	$x_{max}=15$	4·365	8·228	3·863	−0·00852	6·443	−2·2942
	Leone[17]	4·548	8·391	3·843	−0·00851	6·625	−0·3000
4 (top)	$x_{max}=7$	1·115	5·451	4·336	0·01948	3·733	0·2188
	$x_{max}=15$	1·064	5·258	4·194	0·01961	3·771	0·2286
	Leone[17]	1·210	5·492	4·282	0·01880	4·000	0·2375
5 (top)	$x_{max}=7$	—	—	—	—	—	—
	$x_{max}=15$	8·079	9·955	1·876	0·00013	8·957	0·4418
	Leone[17]	8·164	10·215	2·051	0·00020	9·187	0·4500

Table III. Differences between long- and short-domain results for the items listed in Table II

Eddy	Start x^1	Stop x^1	Length	Maximum value	x^1-co-ordinate	x^2-co-ordinate
1 (bottom)	0	0·029	0·029	−0·00001	0·0792	−0·0042
2 (bottom)	0·029	−0·079	−0·108	−0·00362	−0·064	−0·0085
3 (bottom)	−0·138	—	—	−0·00104	−0·168	0·0272
4 (top)	−0·051	−0·193	−0·142	0·00013	0·038	0·0098
5 (top)	—	—	—	—	—	—

CONCLUSIONS

Navier–Stokes flow computations using a primitive variable formulation and the SIMPLE algorithm have been conducted to investigate the effects of downstream open boundary conditions prescribed in a truncated computational domain where inflow occurs through the open boundary. Calculations were performed using staggered and non-staggered grid systems and five different open boundary numerical treatments were considered. The vanishing of the streamwise derivative embodied in OBC1 is an erroneous procedure that amplifies the streamwise component of the velocity at the boundary and decreases the amplitude of the crosswise component. A strong reflection also occurs when linear velocity or temperature extrapolation OBC4 is considered. Results better than those obtained with OBC1 were obtained using OBC2, that is equivalent to expressing the incompressible condition for the velocity at open boundary half-control volume. The monochromatic travelling wave condition, OBC3, produces little reflection and has been shown to be highly suitable to extrapolate vector and scalar fields outside the domain of integration when the flow has a specified mean direction and the travelling wave phase speed can be easily estimated.

The proposed pressure extrapolation condition, OBC5, in the framework of non-staggered grid system and pressure-weighted interpolation method has proven to be an accurate and robust formulation for simulating elliptic flow problems with or without recirculation at the outlet plane.

ACKNOWLEDGEMENTS

The authors gratefully acknowledge Prof. P. M. Gresho for helpful discussions during the Outflow Boundary Condition Minisymposium that took place in Stanford, 14 July 1991.

REFERENCES

1. I. Orlanski, 'A simple boundary condition for unbounded hyperbolic flows', *J. Comput. Phys.*, **21**, 251–269 (1976).
2. R. M. Beam, R. F. Warming and H. C. Yee, 'Stability analysis of numerical boundary conditions and implicit difference approximations for hyperbolic equations', *J. Comput. Phys.*, **48**, 200–222 (1982).
3. K. W. Thompson, 'Time-dependent boundary conditions for hyperbolic systems II', *J. Comput. Phys.*, **89**, 439–461 (1990).
4. Y. Mizuta, 'Generalized boundary conditions on the basis of a deformable-cell method: free surfaces, density interfaces and open boundaries', *Comput. Fluids*, **19**, 377–385 (1991).
5. S. Karni, 'To the boundary and back—a numerical study', *Int. j. numer. methods fluids*, **13**, 201–216 (1991).
6. J. E. Romate, 'Absorbing boundary conditions for free surface waves', *J. Comput. Phys.*, **99**, 135–145 (1992).
7. J. S. Dekruif and A. A. Hassan, 'Implications of truncating semi-infinite physical domains on the accuracy of the solutions to the Navier–Stokes equations', *Comput. and Fluids*, **16**, 133–146 (1985).
8. W. Shyy, 'Numerical outflow boundary conditions for Navier–Stokes flow calculations by a line iterative method', *AIAA J.*, **23**, 1847–1848 (1985).
9. W. Shyy, 'Effects of open boundary on incompressible Navier–Stokes flow computation: numerical experiments', *Numer. Heat Transfer*, **12**, 157–178 (1987).
10. T. Y. Han, J. C. S. Meng and G. E. Innis, 'An open boundary condition for incompressible stratified flows', *J. Comput. Phys.*, **49**, 276–297 (1983).
11. F. Nafat, 'An open boundary condition for the computation of the steady incompressible Navier–Stokes equations', in R. Gruber, J. Periaux and R. P. Shaw (eds), *Proc. 5th Int. Symp. on Numerical Methods in Eng.*, 1989, Vol. 1, pp. 749–756.
12. A. Bottaro, 'Note on open boundary conditions for elliptic flows', *Numer. Heat Transfer (Part B)*, **18**, 243–256 (1990).
13. S. V. Patankar, *Numerical Heat Transfer and Fluid Flow*, Hemisphere, New York, 1980.
14. C. M. Rie and W. L. Chow, 'Numerical study of the turbulent flow past an airfoil with trailing edge separation', *AIAA J.*, **21**, 1525–1532 (1983).
15. M. H. Kobayashi and J. C. F. Pereira, 'Numerical comparison of momentum interpolation methods and pressure–velocity algorithms using non-staggered grids', *Commun. Appl. Numer Methods*, **7**, 173–186 (1991).
16. G. Evans and S. Paulucci, 'The thermoconvective instability of plane Poiseuille flow heated from below: a proposed benchmark solution for open boundary flows', *Int. j. numer. methods fluids*, **11**, 1001–1013 (1990).
17. J. M. Leone Jr., 'Open boundary condition symposium benchmark solution: stratified flow over a backward-facing step', *Int. j. numer. methods fluids*, **11**, 969–984 (1990).
18. B. P. Leonard, 'A stable and accurate convective modelling procedure based on quadratic upstream interpolation', *Comput. methods appl. mech. eng.*, **19**, 59–98 (1979).
19. D. F. G. Durão and J. C. F. Pereira, 'A numerical experimental study of confined unsteady laminar flow around a square obstacle', in C. Taylor, M. G. Habashi and M. Hafez (eds), *Numerical Methods in Laminar and Turbulent Flows*, Pineridge Press, Swansea, 1987, pp. 261–272.
20. H. L. Stone, 'Iterative solution of implicit approximations of multidimensional partial differential equations', *SIAM J. numer. Anal.*, **5**, 530–558 (1968).
21. J. L. T. Azevedo, F. Durst and J. C. F. Pereira, 'Comparison of strongly implicit procedures for the solution of the fluid flow equations in finite difference form', *Appl. Math. Modelling*, **12**, 51–62 (1987).
22. P. M. Gresho and R. L. Sani, 'On pressure boundary conditions for the incompressible Navier–Stokes equations', *Int. j. numer. methods fluids*, **7**, 1111–1145 (1987).
23. L. Quartapelle and M. Napolitano, 'Integral conditions for the pressure in the computation of incompressible viscous flows', *J. Comput. Phys.*, **62**, 340–348 (1986).
24. P. J. Roache, 'A comment on the paper "Finite difference methods for the Stokes and Navier–Stokes equations" by J. C. Strikwerda', *Int. j. numer. methods fluids*, **8**, 1459–1463 (1988).
25. J. L. C. Chang, D. Kwak, S. E. Rogers and R. J. Yang, 'Numerical simulation methods of incompressible flows and an application to the space shuttle main engine', *Int. j. numer. methods fluids*, **8**, 1241–1268 (1988).
26. P. M. Gresho, 'A simple question to SIMPLE users', *Numer. Heat Transfer (Part A)*, **20**, 123 (1991).